

# AU-aware graph convolutional network for Macro- and Micro-expression spotting

Shukang Yin

University of Science and  
Technology of China  
Hefei, Anhui, China  
xjtupanda@mail.ustc.edu.cn

Shiwei Wu

University of Science and  
Technology of China  
Hefei, Anhui, China  
dwustc@mail.ustc.edu.cn

Tong Xu

University of Science and  
Technology of China  
Hefei, Anhui, China  
tongxu@ustc.edu.cn

Shifeng Liu

University of Science and  
Technology of China  
Hefei, Anhui, China  
lsf0619@mail.ustc.edu.cn

Sirui Zhao\*

University of Science and  
Technology of China  
Hefei, Anhui, China  
sirui@mail.ustc.edu.cn

Enhong Chen\*

University of Science and  
Technology of China  
Hefei, Anhui, China  
cheneh@ustc.edu.cn

**Abstract**—Automatic Micro-Expression (ME) spotting in long videos is a crucial step in ME analysis but also a challenging task due to the short duration and low intensity of MEs. When solving this problem, previous works generally lack in considering the structures of human faces and the correspondence between expressions and relevant facial muscles. To address this issue for better performance of ME spotting, this paper seeks to extract finer spatial features by modeling the relationships between facial Regions of Interest (ROIs). Specifically, we propose a graph convolutional-based network, called Action-Unit-aWare Graph Convolutional Network (AUW-GCN). Furthermore, to inject prior information and to cope with the problem of small datasets, AU-related statistics are encoded into the network. Comprehensive experiments show that our results outperform baseline methods consistently and achieve new SOTA performance in two benchmark datasets, CAS(ME)<sup>2</sup> and SAMM-LV. Our code is available at <https://github.com/xjtupanda/AUW-GCN>.

**Index Terms**—Micro-expression, macro-expression, spotting, graph convolutional network, affective computing

## I. INTRODUCTION

Facial expressions highly reflect people’s emotions and convey their psychological states in a non-verbal form [1]. According to intensity and duration, they can be divided into two categories, including Macro-Expression (MaE) and Micro-Expression (ME). Generally, MaEs are more intense and enduring than MEs, usually lasting from 0.5 to 4.0s, and can be faked with intention. In contrast, MEs appear subtle, and their duration is generally less than 0.5s [2]. Moreover, MEs are involuntary, spontaneously manifesting themselves when people try to hide their genuine feelings [3]. In recent years, MEs have been brought to the attention of the research community due to their wide applications, such as criminal investigations [3], clinical psychology [4] and national security [5]. Specifically, an essential part of ME research is ME spotting, which involves locating expression intervals in long untrimmed videos. However, the task is quite

tricky in itself due to the characteristics of ME, i.e., low intensity and short duration.

In recent years, much progress has been made in ME spotting. Previous studies mainly used raw features as input, including RGB images and optical-flow maps. Yap et al. [6] designed RGB sample pairs as model inputs for ME and MaE respectively. However, RGB images are insufficient in characterizing facial movements, especially those of MEs. Therefore, later works such as SOFTNet [7] exploited optical-flow features to describe the subtle motion of facial muscles, and ABPN [8] used finer MDMO [9] features. Nevertheless, by inputting the pre-processed features as a whole into the network, these works did not fully consider the relationships between different parts of human faces as well as the semantic information of these regions. However, this information is crucial to spotting performance because facial expressions appear through the movement of corresponding facial muscle groups, termed Action Units (AUs) [10], and ignorance of this semantic information could bring about confusion and ambiguity in the model. Therefore, this paper proposes to model the relationships between facial ROIs and leverage information of AUs to help extract finer feature representation and boost spotting performance.

To this end, we put forward an AU-aware graph convolutional network (GCN) for spotting MaEs and MEs in long untrimmed videos, dubbed AUW-GCN. Specifically, our model adopts a GCN [11] as the feature embedding backbone to characterize the relationships between different regions on human faces. After that, we modify an ABPN [8] for temporal feature interaction to better utilize contextual information in the videos. Moreover, in an effort to inject prior information about facial expressions and mitigate the issue of over-fitting brought by small datasets, we propose to encode AU statistics into the GCN to capture motion patterns of facial expressions better and achieve finer feature representation. Our main contributions can be summarized as follow:

\*Sirui Zhao and Enhong Chen are corresponding authors.

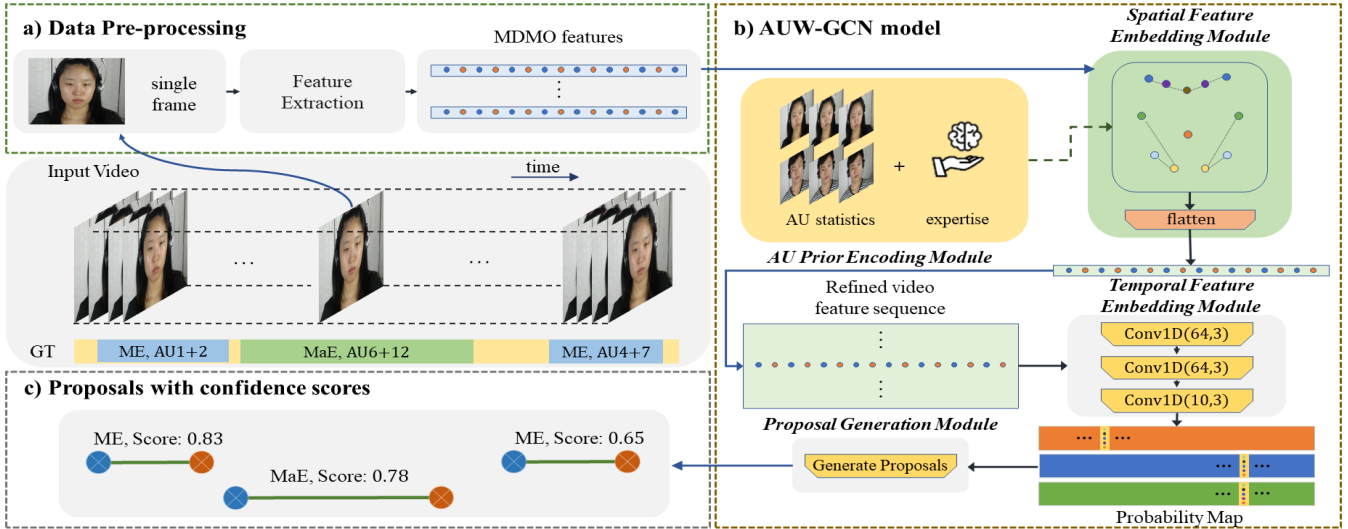


Fig. 1: Illustration of our framework. After feature extraction, we feed MDMO features into SFEM and TFEM to get probability maps, which are later used for proposal generation.

- We propose a model to capture finer spatial features, thus making expression spotting more accurate and complete.
- We design a strategy to encode the prior information about motion patterns of facial expressions into our network, which is crucial to refining spatial feature embedding and alleviating over-fitting.
- We demonstrate the effectiveness of our proposed approach through comprehensive experiments on two standard benchmark datasets, CAS(ME)<sup>2</sup> and SAMM-LV.

## II. RELATED WORKS

### A. ME Spotting

Current methods for the ME Spotting task can be broadly divided into two categories: hand-crafted and deep-learning methods. The former entails hard-wired feature engineering and careful design of signal processing. Specifically, the procedure mainly consists of hand-crafted features design, feature difference analysis, and threshold strategy for determining the intervals of expressions [1]. Typical feature descriptors used in these works include LBP [12], optical-flow [13]–[15] and HOG [16].

With the development of deep learning, automatic feature engineering and end-to-end training have become a possibility. As a result, deep-learning-based methods are raised to a mainstream paradigm. Generally, researchers will choose a standard architecture, including CNNs and RNNs, and treat the task as a typical supervised problem. For example, Wang et al. [2] used 2D-CNNs and 1D-CNNs to extract spatial and temporal features, respectively, with a regression network to refine the interval proposals. Yap et al. [6] adopted 3D-CNNs to extract spatial and temporal features simultaneously. Leng et al. [8] adapted BSN [17] for spotting intervals of ME and MaE flexibly, and we take inspiration from this work to design our network.

### B. Graph Convolutional Network

By treating a human face as a graph with different ROIs as nodes, Liu et al. [18] adopted GCN for AU detection. They built the graph with binary value through setting a threshold on the conditional probability of pairs of AUs. Similarly, Lo et al. [19] used GCN for the ME recognition task. However, applying GCN in ME spotting has been left unexplored. We thus utilize the modelling capacity of GCN and further extend the approach in the field of MaE and ME spotting.

## III. METHODS

Our methods involve feature extraction, the proposed AUW-GCN model, and optimization strategies. The overview of our approach is illustrated in Fig.1.

### A. Feature Extraction

Following [8], the feature extraction procedure includes facial alignment, landmarks detection, optical-flow calculation, and MDMO [9] feature extraction.

Firstly, we use Retinaface [20] to locate the facial bounding box of the first frame in the video and align the subsequent frames to the first one. We denote this aligned video as  $X_V = \{x_n\}_{n=1}^{l_v} \in \mathbb{R}^{H \times W \times l_v}$ , where  $H, W$  are the height and width of a single frame, respectively.  $l_v$  represents the total frame numbers of the video.  $x_n$  is the  $n$ -th frame in the video. After that, we adopt TV-L1 algorithm [21] to compute coarse optical-flow features, denoted as  $O = \{o_n\}_{n=1}^{l_v-1} \in \mathbb{R}^{H \times W \times (l_v-1) \times 2}$ , where  $o_n$  is the  $n$ -th optical-flow map calculated from  $x_n$  and  $x_{n+1}$ . To refine the features, we follow the approach of [9] and choose 12 ROIs and crop them out with facial landmarks detected by SAN [22]. Finally, we compute the finer-grained MDMO features as the model input, denoted as  $F = \{f_n\}_{n=1}^{l_v-1} \in \mathbb{R}^{(l_v-1) \times N \times 2}$ , where  $N=12$  is the number of ROIs.

TABLE I: The detailed architecture of AUW-GCN, following a “backbone-neck-head” design paradigm. RF is the equivalent size of the temporal receptive field. For the GCN layer, we denote the numbers of nodes and hidden dimensions in the form of (N, d).

layer		kernel	stride	dim	RF	act.	output size
<b>Backbone</b>	GCN	-	-	(12,16)	-	relu	$16 \times 12 \times T$
	flatten	-	-	-	-	-	$192 \times T$
<b>Neck</b>	$\text{conv1d}_1^*$	3	1	64	3	relu	$64 \times T$
	$\text{conv1d}_2^*$	3	1	64	7	relu	$64 \times T$
<b>Head</b>	$\text{conv1d}_3^*$	3	1	10	11	-	$10 \times T$

\*: The last two 1D-convolution layers are dilated convolution with a dilation rate set to 2.

## B. AUW-GCN model

As Table I shows, the whole architecture follows a standard detection design paradigm, i.e., backbone, neck, and head. The outputs of our model are preliminary proposals, which are then post-processed to get final spotting results. In this part, we introduce them in sequence, just as how the data flows.

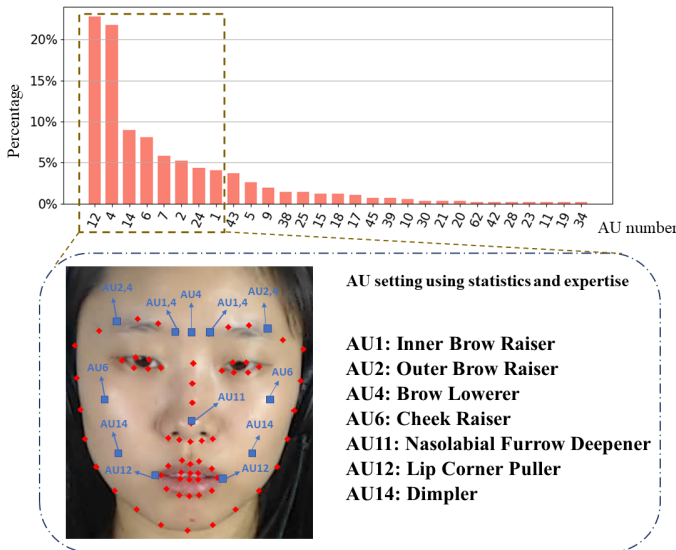


Fig. 2: Illustration of AU selection and correspondence between AUs and ROIs.

1) *AU Prior Encoding Module*: To learn fine-grained relationships in small datasets, we resort to prior information and try to embed this information into GCN. Then naturally, the central problems are how to characterize the correlations of different ROIs and how to build the adjacency matrix. Consequently, we associate co-occurrences with correlations of AUs and map AUs to specific ROIs on human faces. In view of the critical observation that the ratio of AUs follows a long-tailed distribution and some field expertise, we choose 12 ROIs as Fig. 2 shows. Then the remaining problem is how to quantify these relationships in the form of an adjacency matrix. Inspired by [19], we devise a simple yet effective strategy for exploiting AU information in the dataset, which can be encoded as prior belief into our GCN.

For more explicit demonstration, we denote the label set as  $\Phi_g = \{\phi_n = (t_{s,n}, t_{ap,n}, t_{e,n}, \{U_n\})\}_{n=1}^{N_g}$ , where  $N_g$  is the total number of ground-truth labels, each made up of a quadruple, wherein  $t_{s,n}, t_{ap,n}, t_{e,n}$  is the onset, apex, offset frame of the  $n$ -th ground-truth instance  $\phi_n$ , and  $\{U_n\}$  is the set of AUs appearing in the instance. Formally, we construct the adjacency matrix  $A'$  in the following way:

$$A'_{ij} = \sum_{\phi_k} \sum_{i,j} \mathbb{1}(i \in f(U_i), j \in f(U_j)), \quad U_i, U_j \in \{U_k\}. \quad (1)$$

$f(\cdot)$  is a mapping function from a certain AU to a set containing all the corresponding facial regions as shown in Fig 2. We normalize the matrix to get the final adjacency matrix  $A$  to ensure training stability. The adjacency matrix formulated in this way is sparse and efficient but, at the same time, reserves the most representative information.

2) *Spatial Feature Embedding Module*: To characterize the relationships between different parts of human faces and achieve finer spatial feature embedding, we choose GCN as a basic building block for the spatial feature embedding module (SFEM). GCN takes the feature representation matrix  $X \in \mathbb{R}^{d \times N}$  and the adjacency matrix  $A \in \mathbb{R}^{N \times N}$  as input, where  $d$  is the dimension of input features, and  $N$  is the number of nodes of the graph. We can stack  $L$  GCN layers one upon another. The outputs of the  $l$ -th GCN layer can be expressed as:

$$X^l = \sigma(AX^{l-1}W^{l-1}), \quad (2)$$

where we choose ReLU as activation function  $\sigma$ .  $A$  is our prior-encoded adjacency matrix and  $X^{l-1}, W^{l-1}$  are the feature embedding and learnable weight matrix of the  $(l-1)$ -th layer respectively. The input of the module  $X_0 = F$  is the extracted MDMO feature, and the final output  $X^L$  is the refined spatial feature embedding after graph convolution.

3) *Temporal Feature Embedding Module*: This module operates temporal convolution on fine-grained spatial features  $X^L$  from SFEM and outputs probability maps, which can be expressed as:

$$P = \{p_t^s, p_t^{ap}, p_t^e, p_t^{exp}\}, \quad (3)$$

where  $p_t^s, p_t^{ap}, p_t^e, p_t^{exp}$  respectively represent the probability that each frame is classified as an onset, apex, offset, and expression frame. Here we define an expression frame as a frame inside a ground-truth interval. There are two main factors that affect our design choices, the size of the receptive field and the number of parameters. Given the data characteristics, our objective is to design, with a tight budget on model capacity, a model whose temporal receptive field is large enough to incorporate contextual information for mitigating uncertainty. Thus, in order to prevent over-fitting, we use dilated convolution in the last two layers of the module for a lighter architecture.

4) *Proposal Generation Module*: After we get the probability sequences for the onset, apex, and offset frame, we generate candidate proposals as described in Alg. 1.

---

**Algorithm 1:** Generating the candidate proposal set from probability sequences.

---

**Input:** Probability sequences  $p_t^s, p_t^{ap}, p_t^e$ ,  
threshold  $thr_{ap}$ , search range  $k_{dis}$

**Output:** Proposal set  $\Phi_p = \{\phi_i = (\hat{t}_{s,i}, \hat{t}_{e,i}, sc_{p,i})\}_{i=1}^{N_p}$

```

1  $\Phi_p \leftarrow \emptyset$ 
2  $\Phi_p^{ap} \leftarrow \emptyset$ 
3 foreach apex probability  $p_t^{ap} \in p_t^{ap}$  do
4   if  $p_t^{ap} \geq thr_{ap}$  then
5      $\Phi_p^{ap} \leftarrow \Phi_p^{ap} \cup \{i\}$ 
6 foreach apex frame index  $i \in \Phi_p^{ap}$  do
7    $sc_{ap} \leftarrow p_t^{ap}[i]$ 
8    $\hat{t}_s \leftarrow \operatorname{argmax}_{i-k_{dis} \leq t'_s \leq i-1} p_t^s[t'_s]$ 
9    $sc_s \leftarrow p_t^s[\hat{t}_s]$ 
10   $\hat{t}_e \leftarrow \operatorname{argmax}_{i+1 \leq t'_e \leq i+k_{dis}} p_t^e[t'_e]$ 
11   $sc_e \leftarrow p_t^e[\hat{t}_e]$ 
12   $sc_p \leftarrow sc_s \times sc_{ap} \times sc_e$ 
13   $\Phi_p \leftarrow \Phi_p \cup \{(\hat{t}_s, \hat{t}_e, sc_p)\}$ 
14 return  $\Phi_p$ 

```

---

5) *Post processing:* By further processing candidate proposals, we reduce highly-overlapping intervals and thus improve the quality of intervals spotted. The NMS [23] algorithm is adopted to filter out proposals whose scores are lower but are highly overlapped with confident ones, resulting in a final proposal set:  $\Phi'_p = \{\phi_n = (\hat{t}_{s,n}, \hat{t}_{e,n}, sc_{p,n})\}_{n=1}^{N'_p}$ , where  $N'_p$  is the number of final proposals.

### C. Optimization

We convert the spotting task into a common classification problem. Specifically, we devise a binary classification task and a 3-class classification task for different types of frames. To cope with data imbalance, we choose Focal Loss [24] as our basic loss function. Generally, the loss function can be expressed as:

$$L(y, \hat{y}) = -\frac{1}{l_w} \sum_{i=1}^{l_w} \sum_{c=1}^C [\alpha \cdot (1 - y_{i,c})^\gamma \cdot y_{i,c} \cdot \log \hat{y}_{i,c} + (1 - \alpha) \cdot y_{i,c}^\gamma \cdot (1 - y_{i,c}) \cdot \log(1 - \hat{y}_{i,c})], \quad (4)$$

where  $C$  is the number of classes,  $\hat{y}$  is the output probability of the model and  $y$  is the ground-truth label.  $\alpha, \gamma$  are hyper-parameters to balance positive-negative and easy-hard samples, respectively. Note that we use the sliding window technique to segment a long video into snippets, and  $l_w$  is the window size.

## IV. EXPERIMENTS

### A. Experimental Settings

Following the protocol of MEGC2021 [27], we employ the Leave-One-Subject-Out (LOSO) cross-validation strategy for our experiments.

**Datasets.** We validate our methods and conduct experiments on two benchmark datasets: CAS(ME)<sup>2</sup> [28] dataset has 98 annotated videos from 22 subjects with 30 fps and 357 ground-truth instances, including 57 ME labels and 300 MaE labels; SAMM-LV [29] is a dataset of 224 long videos with 200fps recorded from 32 subjects. The dataset contains 159 ME samples and 343 MaE samples.

**Implementation Details.** The model is trained by Adam optimizer on both datasets for 100 epochs with a learning rate of 0.01. The thresholds for apex score and NMS post-processing are set to 0.4 and 0.5, respectively.

**Evaluation Metrics.** We follow the standard evaluation protocol used in the MEGC2021 spotting track. A proposal is considered a True-Positive (TP) if it satisfies the following:

$$\frac{W_{proposal} \cap W_{GroundTruth}}{W_{proposal} \cup W_{GroundTruth}} \geq k_{IoU}, \quad (5)$$

where  $k_{IoU}$  is set to 0.5 officially. Otherwise, the proposal counts as a False-Positive (FP). We calculate precision, recall, and F1-score for a more comprehensive comparison against other methods.

### B. Experimental Results

**Overall Results.** We report the performance of our methods on MEGC2021 benchmarks: CAS(ME)<sup>2</sup> and SAMM-LV, and comprehensively compare our results with hand-crafted methods and deep-learning methods by following [1]. The results are listed in Table II. As the table shows, our methods outperform others consistently on both datasets, especially on SAMM-LV. Our overall f1-score reaches 0.3653 on CAS(ME)<sup>2</sup> and 0.3706 on SAMM-LV. This is the first time that deep-learning methods beat SOTA hand-crafted method, OF-FD [14]. Though our performance on ME is lower, it should be noted that the latter requires laborious feature engineering and heavy tuning of parameters, while our methods can adaptively learn fine-grained feature embedding and exempt the chore of complicated tuning. Moreover, deep-learning methods excel in generalization, which is a promising prospect with the fast development of new and larger datasets. **Ablation Studies.** To further verify the effectiveness of our proposed methods, we conduct empirical studies on the components of our model based on the CAS(ME)<sup>2</sup> dataset.

To verify the effectiveness of introducing GCN for better spatial feature embedding, we compare the results of the model with and without GCN as Table III shows. It is clear that introducing the SFEM improves all the metrics consistently. Specifically, the F1-score rises from 0.3174 to 0.3318. This improvement verifies the effectiveness of our proposed module in refining the feature embedding. Moreover, applying AU-prior encoding into the module brings another 10.0% boost in F1-score and achieves a higher recall by 14.2%. The enhancement validates the efficacy of our strategy for building an adjacency matrix from prior belief. This can be partially explained by the fact that given a small dataset, learning relationships between graph node embedding could be pretty tricky, and may even fall into over-fitting. In contrast, by

TABLE II: Spotting results on CAS(ME)<sup>2</sup> and SAMM-LV datasets in terms of F1-score

Methods		CAS(ME) <sup>2</sup>			SAMM Long Videos			Overall
		MaE	ME	Overall	MaE	ME	Overall	
Hand-crafted methods	MDMD [13]	0.1196	0.0082	0.0376	0.0629	0.0364	0.0445	0.0445
	SP-FD [15]	0.2131	0.0547	0.1403	0.0725	0.1331	0.0999	0.1243
	OF-FD [14]	0.3782	<b>0.1965</b>	0.3436	0.4149	<b>0.2162</b>	0.3638	0.3534
Deep-learning methods	SOFTNet [7]	0.2410	0.1173	0.2022	0.2169	0.1520	0.1881	0.3006
	3D-CNN [6]	0.2145	0.0714	0.1675	0.1595	0.0466	0.1084	-
	Concat-CNN [25]	0.2505	0.0153	0.2019	0.3553	0.1155	0.2736	0.2452
	LSSNet [26]	0.3770	0.0420	0.3250	0.2810	0.1310	0.2380	0.2717
	MTSN [1]	0.4104	0.0808	0.3620	0.3459	0.0878	0.2867	0.3191
	<b>AUW-GCN (Ours)</b>	<b>0.4235</b>	0.1538	<b>0.3834</b>	<b>0.4293</b>	0.1984	<b>0.3728</b>	<b>0.3771</b>

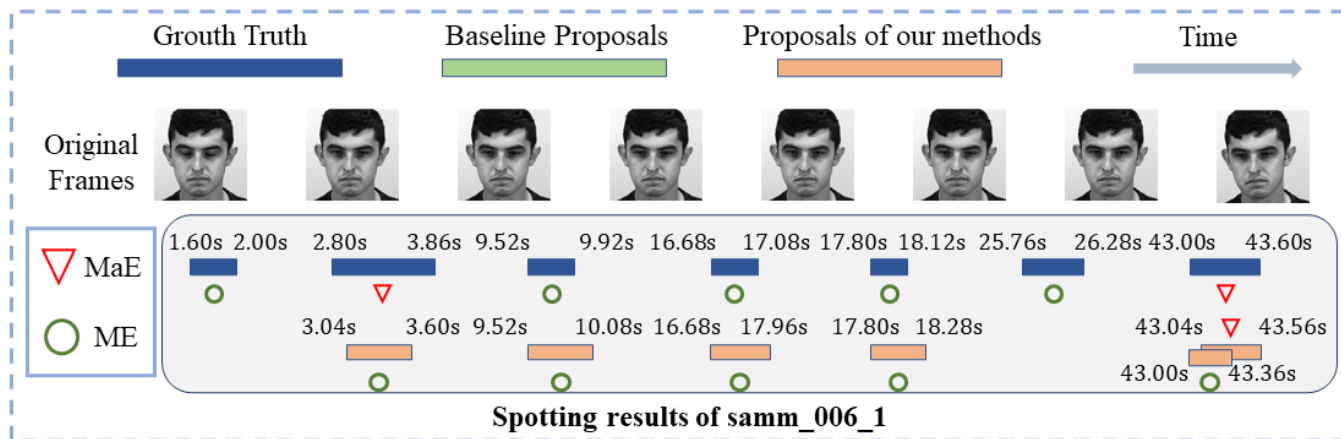


Fig. 3: Visualization analysis of spotting results. The example is from video samm\_006\_1 on SAMM-LV dataset.

TABLE III: Study of the effectiveness of SFEM and contribution of each component in the module, i.e., GCN and Prior encoding. Note that without prior, the GCN learns the adjacency matrix from data through training.

GCN	Prior	Precision	Recall	F1-score
✗	✗	0.3527	0.2885	0.3174
✓	✗	0.3804	0.2941	0.3318
✓	✓	<b>0.4000</b>	<b>0.3361</b>	<b>0.3653</b>

injecting specific knowledge into the model, the network can learn correlations between nodes more efficiently.

TABLE IV: The results of ablation study on model design choices. NL = number of GCN layers. ND = hidden dimension of GCN.

Setting	NL	ND	Precision	Recall	F1-score
a	1	16	<b>0.4000</b>	<b>0.3361</b>	<b>0.3653</b>
b	1	32	0.1025	0.1625	0.1257
c	2	16	0.3869	0.2969	0.3360
d	2	32	0.0850	0.1092	0.0956

We also investigate the effects of different model capacities by varying the number of layers and hidden dimensions as listed in Table IV. Compared with setting (a), setting (b) doubles the hidden dimension and results in severe perfor-

mance degradation. Moreover, increasing both the number of layers and hidden dimension (setting (d)) causes a drop in the F1-score from 0.3653 to 0.0956. In contrast, only adjusting the number of GCN layers (setting (c)) brings a slight degradation. These results overall suggest that larger capacity is inappropriate for small datasets, and our model design is better suited.

### C. Case Study

For an intuitive illustration, we show a qualitative example in Fig. 3. As the figure shows, our model can generate proposals with high recall for both MaEs and MEs owing to the temporal modeling capacity of TFEM. The result suggests that leveraging contextual information can help the model locate more accurate and complete intervals.

## V. CONCLUSIONS

This paper proposed a graph-based network for spotting MaEs and MEs, dubbed AUW-GCN. To assist the model in learning relationships between different regions of human faces, a strategy was devised for injecting AU-prior information through careful design of the adjacency matrix of the GCN module. Moreover, comprehensive experiments on two benchmark datasets demonstrated our methods' superior effectiveness and generalization ability.

## REFERENCES

- [1] Gen Bing Liong, Sze-Teng Liong, John See, and Chee-Seng Chan, "Mtsn: A multi-temporal stream network for spotting facial macro-and micro-expression with hard and soft pseudo-labels," in Proceedings of the 2nd Workshop on Facial Micro-Expression: Advanced Techniques for Multi-Modal Facial Expression Analysis, 2022, pp. 3–10.
- [2] Su-Jing Wang, Ying He, Jingting Li, and Xiaolan Fu, "Mesnet: A convolutional neural network for spotting multi-scale micro-expression intervals in long videos," IEEE Transactions on Image Processing, vol. 30, pp. 3956–3969, 2021.
- [3] Paul Ekman, Telling lies: Clues to deceit in the marketplace, politics, and marriage (revised edition), WW Norton & Company, 2009.
- [4] Frank Salter, Karl Grammer, and Anja Rikowski, "Sex differences in negotiating with powerful males," Human Nature, vol. 16, no. 3, pp. 306–321, 2005.
- [5] Yee-Hui Oh, John See, Anh Cat Le Ngo, Raphael C-W Phan, and Vishnu M Baskaran, "A survey of automatic facial micro-expression analysis: databases, methods, and challenges," Frontiers in psychology, vol. 9, pp. 1128, 2018.
- [6] Chuin Hong Yap, Moi Hoon Yap, Adrian Davison, Connah Kendrick, Jingting Li, Su-Jing Wang, and Ryan Cunningham, "3d-cnn for facial micro-and macro-expression spotting on long video sequences using temporal oriented reference frame," in Proceedings of the 30th ACM International Conference on Multimedia, 2022, pp. 7016–7020.
- [7] Gen-Bing Liong, John See, and Lai-Kuan Wong, "Shallow optical flow three-stream cnn for macro-and micro-expression spotting from long videos," in 2021 IEEE International Conference on Image Processing (ICIP). IEEE, 2021, pp. 2643–2647.
- [8] Wenhao Leng, Sirui Zhao, Yiming Zhang, Shiifeng Liu, Xinglong Mao, Hao Wang, Tong Xu, and Enhong Chen, "Abpn: Apex and boundary perception network for micro-and macro-expression spotting," in Proceedings of the 30th ACM International Conference on Multimedia, 2022, pp. 7160–7164.
- [9] Yong-Jin Liu, Jin-Kai Zhang, Wen-Jing Yan, Su-Jing Wang, Guoying Zhao, and Xiaolan Fu, "A main directional mean optical flow feature for spontaneous micro-expression recognition," IEEE Transactions on Affective Computing, vol. 7, no. 4, pp. 299–310, 2015.
- [10] Erika L Rosenberg and Paul Ekman, What the face reveals: Basic and applied studies of spontaneous expression using the Facial Action Coding System (FACS), Oxford University Press, 2020.
- [11] Thomas N Kipf and Max Welling, "Semi-supervised classification with graph convolutional networks," arXiv preprint arXiv:1609.02907, 2016.
- [12] Antti Moilanen, Guoying Zhao, and Matti Pietikäinen, "Spotting rapid facial movements from videos using appearance-based feature difference analysis," in 2014 22nd international conference on pattern recognition. IEEE, 2014, pp. 1722–1727.
- [13] Ying He, Su-Jing Wang, Jingting Li, and Moi Hoon Yap, "Spotting macro-and micro-expression intervals in long video sequences," in 2020 15th IEEE International Conference on Automatic Face and Gesture Recognition (FG 2020). IEEE, 2020, pp. 742–748.
- [14] He Yuhong, "Research on micro-expression spotting method based on optical flow features," in Proceedings of the 29th ACM International Conference on Multimedia, 2021, pp. 4803–4807.
- [15] Li-Wei Zhang, Jingting Li, Su-Jing Wang, Xian-Hua Duan, Wen-Jing Yan, Hai-Yong Xie, and Shu-Cheng Huang, "Spatio-temporal fusion for macro-and micro-expression spotting in long video sequences," in 2020 15th IEEE International Conference on Automatic Face and Gesture Recognition (FG 2020). IEEE, 2020, pp. 734–741.
- [16] Adrian Davison, Walied Merghani, Cliff Lansley, Choon-Ching Ng, and Moi Hoon Yap, "Objective micro-facial movement detection using facs-based regions and baseline evaluation," in 2018 13th IEEE international conference on automatic face & gesture recognition (FG 2018). IEEE, 2018, pp. 642–649.
- [17] Tianwei Lin, Xu Zhao, Haisheng Su, Chongjing Wang, and Ming Yang, "Bsn: Boundary sensitive network for temporal action proposal generation," in Proceedings of the European conference on computer vision (ECCV), 2018, pp. 3–19.
- [18] Zhilei Liu, Jiahui Dong, Cuicui Zhang, Longbiao Wang, and Jianwu Dang, "Relation modeling with graph convolutional networks for facial action unit detection," in International Conference on Multimedia Modeling. Springer, 2020, pp. 489–501.
- [19] Ling Lo, Hong-Xia Xie, Hong-Han Shuai, and Wen-Huang Cheng, "Mer-gcn: Micro-expression recognition based on relation modeling with graph convolutional networks," in 2020 IEEE Conference on Multimedia Information Processing and Retrieval (MIPR). IEEE, 2020, pp. 79–84.
- [20] Jiankang Deng, Jia Guo, Evangelos Ververas, Irene Kotsia, and Stefanos Zafeiriou, "Retinaface: Single-shot multi-level face localisation in the wild," in Proceedings of the IEEE/CVF conference on computer vision and pattern recognition, 2020, pp. 5203–5212.
- [21] Christopher Zach, Thomas Pock, and Horst Bischof, "A duality based approach for realtime tv-l 1 optical flow," in Joint pattern recognition symposium. Springer, 2007, pp. 214–223.
- [22] Xuanyi Dong, Yan Yan, Wanli Ouyang, and Yi Yang, "Style aggregated network for facial landmark detection," in Proceedings of the IEEE Conference on Computer Vision and Pattern Recognition, 2018, pp. 379–388.
- [23] Alexander Neubeck and Luc Van Gool, "Efficient non-maximum suppression," in 18th International Conference on Pattern Recognition (ICPR'06). IEEE, 2006, vol. 3, pp. 850–855.
- [24] Tsung-Yi Lin, Priya Goyal, Ross Girshick, Kaiming He, and Piotr Dollár, "Focal loss for dense object detection," in Proceedings of the IEEE international conference on computer vision, 2017, pp. 2980–2988.
- [25] Bo Yang, Jianming Wu, Zhiguang Zhou, Megumi Komiya, Koki Kishimoto, Jianfeng Xu, Keisuke Nonaka, Toshiharu Horiuchi, Satoshi Komorita, Gen Hattori, et al., "Facial action unit-based deep learning framework for spotting macro-and micro-expressions in long video sequences," in Proceedings of the 29th ACM International Conference on Multimedia, 2021, pp. 4794–4798.
- [26] Wang-Wang Yu, Jingwen Jiang, and Yong-Jie Li, "Lssnet: A two-stream convolutional neural network for spotting macro-and micro-expression in long videos," in Proceedings of the 29th ACM International Conference on Multimedia, 2021, pp. 4745–4749.
- [27] Jingting Li, Moi Hoon Yap, Wen-Huang Cheng, John See, Xiaopeng Hong, Xiaobai Li, and Su-Jing Wang, "Fme'21: 1st workshop on facial micro-expression: Advanced techniques for facial expressions generation and spotting," in Proceedings of the 29th ACM International Conference on Multimedia, 2021, pp. 5700–5701.
- [28] Fangbing Qu, Su-Jing Wang, Wen-Jing Yan, He Li, Shuhang Wu, and Xiaolan Fu, "Cas(me)<sup>2</sup>: a database for spontaneous macro-expression and micro-expression spotting and recognition," IEEE Transactions on Affective Computing, vol. 9, no. 4, pp. 424–436, 2017.
- [29] Chuin Hong Yap, Connah Kendrick, and Moi Hoon Yap, "Samm long videos: A spontaneous facial micro-and macro-expressions dataset," in 2020 15th IEEE International Conference on Automatic Face and Gesture Recognition (FG 2020). IEEE, 2020, pp. 771–776.